# Spectral form factors of topological phases

Anurag Sarkar,[*] Subrata Pachhal,[†] Adhip Agarwala,[‡] and Diptarka Das[§]
*Department of Physics, Indian Institute of Technology, Kanpur 208016, India*

(Received 15 August 2023; revised 10 February 2024; accepted 18 March 2024; published 9 April 2024)

Signatures of dynamical quantum phase transitions and chaos can be found in the time evolution of generalized partition functions such as spectral form factors (SFF) and Loschmidt echoes. While a lot of work has focused on the nature of such systems in a variety of strongly interacting quantum theories, in this work, we study their behavior in short-range entangled topological phases, particularly focusing on the role of symmetry-protected topological zero modes. We show, using both analytical and numerical methods, how the existence of such zero modes in any representative system can mask the SFF with large period (akin to generalized Rabi) oscillations, hiding any behavior arising from the bulk of the spectrum. Moreover, in a quenched disordered system, these zero modes fundamentally change the late-time universal behavior reflecting the chaotic signatures of the zero-energy manifold. Our study uncovers the rich physics underlying the interplay of chaotic signatures and topological characteristics in a quantum system.

DOI: 10.1103/PhysRevB.109.155126

## I. INTRODUCTION

Ideas of thermalization and chaos have become pervasive in multiple subdisciplines of physics, including classical and quantum many-body systems, quantum field theory, gravity, and fluids [1–10]. These questions become crucial for understanding the phases of interacting quantum systems when they are either driven or coupled to baths; however, methods of characterizing chaos are few and limited. The behavior of the spectral form factor (SFF) in such systems has been particularly illuminating. Most interestingly, one finds that SFFs and their generalizations, such as the Loschmidt echo [11] and Fisher zeros [12,13], follow universal features independent of underlying microscopic details. It is known that interacting many-body chaotic systems show a dip-linear ramp structure in the SFF, which saturates at late times [14,15]. This behavior, however, has intriguing microstructures which depend on the underlying symmetries, nature of interactions, dimensionality, and localization properties [11]. The SFF was also recently investigated even in noninteracting systems to decipher signatures of single-particle chaos [16,17] and in field theories to determine the signatures of a critical point [10,18]. This led to interesting connections between a host of phenomena from diverse physics areas. However, the behavior of the SFF vis-à-vis the topological properties of a quantum Hamiltonian is little explored.

In this paper, we investigate the behavior of the SFF in symmetry-protected topological systems. Here, phases are characterized by topological invariants, which are protected by discrete symmetries [19–23]. A paradigmatic topological model is the Su-Schrieffer-Heeger (SSH) model [24], in which the system hosts chiral symmetry-protected edge modes in the topological phase. We show that the existence of such zero-dimensional topologically protected eigenstates can fundamentally transform the SFF, exhibiting large time oscillations. We find, both numerically and analytically, that they are generalizations of Rabi oscillations, in which the SFF locks between a few states of the complete many-body spectrum. We further show that this holds even in higher-order topological insulator (HOTI) phases [25], where a $d$-dimensional topological phase hosts $(d-2)$-dimensional boundary modes.

Given the quadratic nature of the Hamiltonians, our study also adds to the emerging area of understanding one-body chaos, recently explored in Sachdev-Ye-Kitaev (SYK-2) [16,17] and in strongly coupled free gauge theories [26]. In order to explore signatures of one-body chaos and its interplay with topological order, we study a variant of the SSH model in which a subregion of the bulk is randomized with all-to-all hoppings while keeping the edge protected. The SFF, in this case, shows a dip followed by an early-time oscillating exponential ramp reminiscent of one-body chaos in SYK-2 [16]. This develops into an intermediate linear ramp that plateaus at late times in both the trivial and topological phases. In the topological phase, while, for any representative configuration, at late times there are Rabi oscillations, under ensemble averaging, these oscillations get destroyed given the random phase lags between various Rabi modes. This reflects the non-self-averaging characteristic of the SFF [27] in topological, yet disordered, systems. Interestingly, this averaged asymptotic value in the topological phase is different from that in the trivial phase and depends only on the random matrix properties of the zero-energy manifold. We end the paper with a perspective on how the interplay between topological features and chaotic signatures may be a rich playground to uncover a host of new phenomena in both lattice and field-theoretic quantum many-body systems.

This paper is organized in the following way: in Sec. II, we discuss the general definition of the SFF for a many-body

[*]sarkara@iitk.ac.in
[†]pachhal@iitk.ac.in
[‡]adhip@iitk.ac.in
[§]didas@iitk.ac.in

 

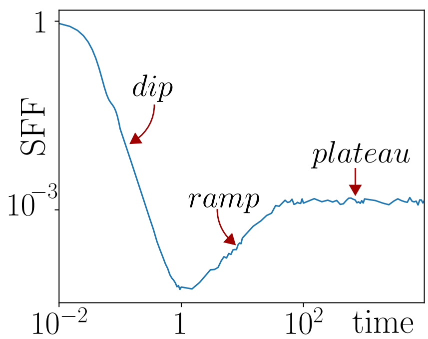


FIG. 1. The ensemble-averaged SFF for a Gaussian unitary ensemble with $1000 \times 1000$ matrices, denoting the dip, linear ramp, and plateau.

chaotic system and for a free-fermionic eigenspectrum. In Sec. III, we study the feature of the SFF in topological Hamiltonians, in particular with the presence of zero-dimensional boundary modes in the system. Then, we discuss how the SFF behaves in a topological phase with a "chaotic" bulk-disordered background in Sec. IV. We provide an intuitive understanding of our results by introducing an effective toy model and, in parallel, by using random matrix theory results. We provide a summary of the results and conclude in Sec. V. The stability of the disordered system and some detailed calculations are provided in Appendixes A and B.

## II. SPECTRAL FORM FACTOR

In general, the SFF of a system is defined as

$$\mathrm{SFF}(\beta, t) \equiv \mathcal{Z}_2(\beta, t) = \frac{Z(\beta + it)Z(\beta - it)}{Z(\beta)^2}, \qquad (1)$$

where $\beta$ and $t$ are the inverse temperature and real time, respectively. $Z(\beta + it)$ denotes the generalized partition function. In terms of the many-body energy eigenstates $E_n$, we can then write

$$\mathcal{Z}_2(\beta, t) = \frac{1}{Z^2} \sum_{m,n} e^{-\beta(E_m+E_n)} e^{it(E_m-E_n)}, \qquad (2)$$

where $Z(\beta + it) = \sum_n e^{-(\beta+it)E_n}$. For a many-body chaotic system, $\mathcal{Z}_2(\beta, t)$ has distinct regions as a function of $t$. Starting from $t = 0$, it has a power law decay until a particular time $t = t_{\mathrm{dip}}$ (dip time), at which the SFF attains its minima. For the chaotic system with $N$ many-body energy states, $t_{\mathrm{dip}} \sim \sqrt{N}$ [28]. After this point the connected part of the SFF starts to become important, and the SFF starts to take the universal random matrix ensemble form manifested as a linear growth of the SFF with time. This region is denoted as the "ramp." The ramp ends at $t = t_{\mathrm{plateau}} \sim N$, denoted as the plateau time or the Heisenberg time. This timescale scales as the inverse of the average level spacing of the system; thus, after this point the discreteness of the energy spectrum becomes important. The SFF saturates after $t_{\mathrm{plateau}}$ and is denoted as the "plateau" [29,30]. This linear ramp is denoted as a characteristic feature of a many-body chaotic interacting system [14,15] (see Fig. 1, where the SFF is plotted for a random matrix drawn out of a Gaussian unitary ensemble (GUE) [14,31,32]). On the contrary, the SFF in an integrable system does not show such a ramp; the SFF in this case decays and then immediately plateaus.

In a noninteracting fermionic system, given a set of single-particle eigenvalues $\epsilon_n$, the generalized partition function is given by

$$Z(\beta + it) = \prod_n \{1 + \exp[-(\beta + it)\epsilon_n]\}, \qquad (3)$$

where $n \in 0, \dots, L-1$ and $L$ is the system size. Thus, for a symmetric eigenspectrum ($\epsilon_n \longleftrightarrow -\epsilon_n$), the SFF [see Eq. (1)] can be written as

$$\mathcal{Z}_2(\beta, t) = \prod_{\epsilon_n > 0} Z_2^{\epsilon_n}(\beta, t) = \prod_{\epsilon_n > 0} \frac{[\cosh(\beta\epsilon_n) + \cos(\epsilon_n t)]^2}{[1 + \cosh(\beta\epsilon_n)]^2}, \qquad (4)$$

which implies that the real-time behavior takes a highly convoluted form dependent on the frequencies of the single-particle energies.

From (2), it may then appear that the time-averaged value is $\sim Z(2\beta)/Z(\beta)^2$ on general grounds. Our results point out that even in an otherwise dense spectrum, the existence of topologically protected zero modes may render this asymptotic value insignificant and mask it with generalized oscillations. To elaborate this further, we now look into the features of the SFF in some specific symmetry-protected topological models.

## III. MODEL

To study the behavior of the SFF in the symmetry-protected topological phase, we first consider the paradigmatic SSH model [24], in which spinless fermions hop in a one-dimensional chain via the following Hamiltonian:

$$H_{\mathrm{SSH}} = -\sum_i (v c_{iA}^\dagger c_{iB} + w c_{iB}^\dagger c_{i+1,A} + \mathrm{H.c.}), \qquad (5)$$

where $c_{i\alpha}^\dagger$ ($c_{i\alpha}$) is the fermionic creation (annihilation) operator at site $i$ for the orbitals $\alpha \equiv A, B$ and $v$ and $w$ are the intra- and interunit cell hopping strengths, respectively. The system has time-reversal and sublattice symmetries, restricting it to the BDI symmetry class, which realizes general off-diagonal real matrices of the free-fermion tenfold classification [33,34], such that the system spectra are always symmetric about energy $E = 0$. The bulk spectrum of the model is given by $E(k) = \pm\sqrt{v^2 + w^2 + 2vw\cos k}$, where $k$ is the discrete momentum of the periodic chain. At half filling (i.e., pinning the Fermi energy at $E_F = 0$), by tuning $v/w$, the system goes from one insulator to another insulator via the quantum critical point $|v/w| = 1$. The insulating phase in the $|v/w| < 1$ regime is topological and characterized by a nontrivial winding number of the bulk band; the corresponding open chain hosts two close to zero energy modes at the boundary with an edge localization length $\xi = [\ln(|w/v|)]^{-1}$. To see the feature in the SFF with an underlying symmetry-protected topology, throughout this article we consider an open SSH chain so that the spectrum contains boundary-localized zero-energy modes.

In the trivial region ($|v| > |w|$), for all values of $\beta$, the SFF $\mathcal{Z}_2(\beta, t)$ is a superposition of all the single-particle energies [see Eq. (4)], thus resulting in a convoluted noisy oscillation. This is rather uninteresting, as can be seen by the behavior

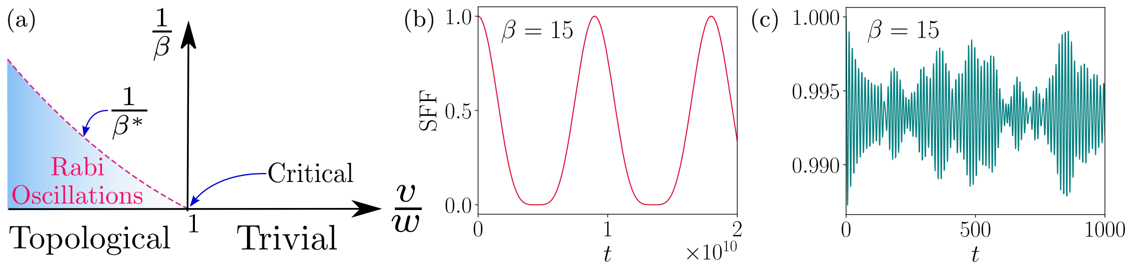


FIG. 2. (a) A topological phase achieved in a Hamiltonian system [see Eq. (5) for the SSH model] is tuned by a parameter $v/w$. This sets the energy scale $T^* = \frac{1}{\beta^*}$ (shown by the dashed line) below which the system shows prominent oscillations in its SFF, as in (b) (with $L = 60$, $v/w = 0.5$, $\beta = 15$). (c) The same system in the trivial region ($v/w = 2$) shows no signs of such oscillations.

of the SFF in the trivial region with $v/w = 2$ [Fig. 2(c)]. However, in the topological regime, an interesting behavior emerges when boundary modes, whose energy $\epsilon_1 \to 0$ exponentially in system size, dominate. This results in a timescale $\sim\pi/\epsilon_1$, where the SFF first goes to zero and then oscillates with the same frequency, drowning all noisy behavior due to higher-energy modes which are exponentially killed due to a finite $\beta$ [see Fig. 2(b), the $v/w = 0.5$ topological region]. These long-time oscillations can be understood as generalized Rabi oscillations, which we now explore further.

### A. Rabi oscillations

In general, given any initial state of a two-level system, the way the probability density of the state oscillates under time evolution is known as Rabi oscillation. While generally discussed in the context of a time-dependent perturbation, even for a constant perturbation switched on at $t = 0$, the overlap of the unperturbed eigenstates with the time-evolved state oscillates with a characteristic frequency decided by the energy gap of the two-level system [35,36]. We next show that the oscillations in the SFF can be understood as exactly these oscillations for a generalized initial state.

We now discuss that the long-time oscillations of the SFF are, in fact, generalized Rabi oscillations, where the system locks between the boundary modes. Consider a wave function which is an equal superposition of *all* the many-body basis states,

$$|\Psi\rangle = \frac{1}{2^L}\sum_{\{N_n\}} |\{N_n\}\rangle, \tag{6}$$

where $|\{N_n\}\rangle$ specifies the Fock state representation labeled by occupancies ($N_n = 0, 1$) of the single-particle state $|\psi_n\rangle$ with eigenenergy $\epsilon_n$. When "quenched" with the Hamiltonian, its fidelity at a later time is

$$\mathcal{F}(t) = \langle\Psi|\Psi(t)\rangle \propto Z(it). \tag{7}$$

Thus, instances where $Z(t) \to 0$ are Rabi oscillations of a pure state under time evolution. At $\beta = 0$, the fidelity behavior will be uncharacteristic because all $\epsilon_n$ will show convoluted oscillations.

However, at a finite temperature, the initial state [see Eq. (6)] can be generalized to

$$|\Psi(\beta)\rangle \propto \sum_{\{N_n\}} \exp(-\beta E_{\{N_n\}}/2)|\{N_n\}\rangle. \tag{8}$$

When evolved in time, the corresponding fidelity is $Z(\beta + it)/Z(\beta)$, and thus, the SFF is just $|\mathcal{F}|^2$. Hence, SFF $\to 0$ are essentially the zeros of the Rabi oscillations of $|\Psi(\beta)\rangle$. Note that there is no external driving in the system; rather, the Hamiltonian evolution itself acts like a "drive" engineering the oscillations from the parent state $|\Psi(\beta)\rangle$. Given the states are normalized by the thermal occupancy factors, the states with the largest weights are where $N_n = 1\,\forall\,\epsilon_n < 0$. In a periodic system, this isolates a single state; however, in an open one-dimensional SSH chain, when in the topological phase, this results in *four* states which are exponentially close in their many-body energies. They correspond to different ways of occupying the (right and left) boundary modes ($\equiv |R\rangle, |L\rangle$). Thus,

$$|\Psi(\beta,t)\rangle \sim \tfrac{1}{2}\big(|\circ\circ\rangle + e^{-(\frac{\beta}{2}+it)\epsilon_a}|*\circ\rangle + e^{-(\frac{\beta}{2}+it)\epsilon_b}|\circ *\rangle + |**\rangle\big) \otimes |N_n = 1\,\forall\,\epsilon_n < 0\rangle, \tag{9}$$

where $\epsilon_a$ and $\epsilon_b$ ($\epsilon_b = -\epsilon_a$) represent the antibonding and bonding orbitals combined out of the left and right edge states ($\{|b\rangle, |a\rangle\} = \frac{1}{\sqrt{2}}(|R\rangle \pm |L\rangle)$ and $*$ ($\circ$) represents their occupancies (vacancies) in the $|n_a, n_b\rangle$ basis. Because of the bulk gap $\Delta_g \sim |w - v|$ between the valence and conduction bands, other states get exponentially damped by $\sim\exp(-\beta\Delta_g)$. This introduces a temperature scale $T^* \sim \frac{1}{\beta^*} = \Delta_g$, below which the Rabi oscillations are strong. For $T > \Delta_g$, these Rabi oscillations dissolve with the bulk signatures. As is clear, the Rabi oscillation period is determined by edge mode energies $\sim\frac{\pi}{\epsilon_a}$. Unlike a single qubit, in this case, the SFF behaves as

$$\mathrm{SFF}(t) \sim [1 + \cos(\epsilon_a t)]^2. \tag{10}$$

Thus, the rise from the minimum is $\propto t^4$ [see Fig. 4(d) below].

In Fig. 3, we show the behavior of the SFF at the trivial, topological, and critical points on the $\{\beta, t\}$ plane. We see that the zeros of the SFF disappear for small values of $\beta$ in the trivial phase, while in the topological phase, the zeros persist even for high $\beta$. This denotes that the topological phase [see Fig. 3(b)] has dominant oscillations.

From Eq. (10), the oscillations have a time period $\sim\pi/\epsilon_a$. As for an SSH chain of length $L$, the zero energies scale as $\epsilon_a \sim \exp(-L\ln|\frac{w}{v}|)$, and the time period scales as $\sim\pi\exp(-L\ln|\frac{v}{w}|)$. The SFF starts from its maximum at $t = 0$ and attains its first zero minimum at the half time period $\sim\pi\exp(-L\ln|\frac{v}{w}|)$ [see Fig. 2(b)]. Thus, the subsequent

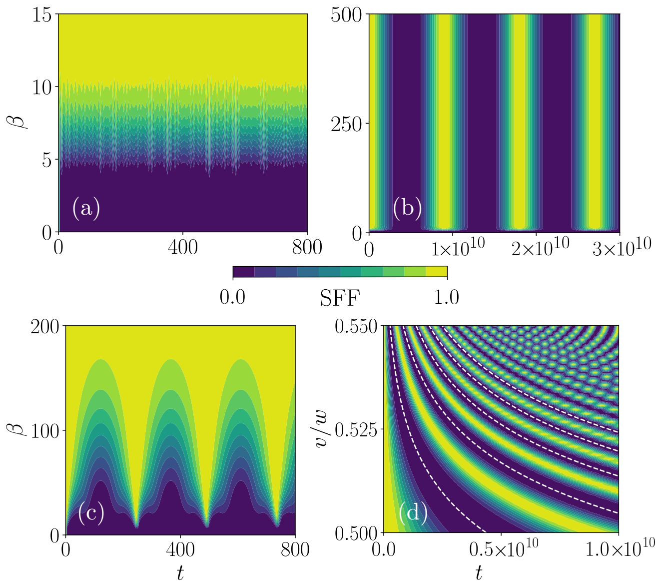


FIG. 3. Contour plot of SFF in the $\beta$-$t$ plane for an open boundary SSH model ($L = 60$) (a) in the trivial regime with $v = 1$ and $w = 0.5$, (b) in the topological regime with $v = 0.5$ and $w = 1$, and (c) at the critical point with $v = 0.5$ and $w = 0.5$. (d) Behavior of the SFF in the $v/w$-$t$ plane for $\beta = 30$. The dashed lines are analytical curves denoting the zeros of the SFF (see text).

minima appear at the odd multiples of this half period; we denote these points as $t_{\text{Rabi}} \sim (2k - 1)\pi \exp(-L \ln |\frac{v}{w}|)$, with $k \in \mathbb{Z}^+$. Numerically, the exact expression can be obtained as

$$t_{\text{Rabi}} = 2.653(2k - 1)\pi \exp\left[-0.483\, L \ln\left(\left|\frac{v}{w}\right|\right)\right]. \quad (11)$$

This expression is consistent with the behavior of the SFF in the topological phase, as can be seen in Fig. 3(d) when plotted on the $v/w, t$ plane.

### B. HOTI phase

In order to further investigate the behavior of the SFF in the presence of topologically protected zero-dimensional boundary modes, we now focus on a HOTI model in which spinless electrons on a square lattice host four corner states [25]. The Bloch Hamiltonian of the model is a four-band insulator given by

$$H(k) = [\gamma + \lambda \cos(k_x)]\Gamma_4 + \lambda \sin(k_x)\Gamma_3 + [\gamma + \lambda \cos(k_y)]\Gamma_2 + \lambda \sin(k_y)\Gamma_1, \quad (12)$$

where $\Gamma_i = -\tau_2\sigma_i$ for $i = 1, 2, 3$ and $\Gamma_4 = \tau_1\sigma_0$; $\sigma$ and $\tau$ are Pauli matrices which act on the four orbitals of a unit cell. The model preserves both time-reversal and charge-conjugation symmetry, so it belongs to the BDI symmetry class, like the SSH model. The bulk energies of the Hamiltonian are given by $E(k) = \pm\sqrt{2\lambda^2 + 2\gamma^2 + 2\gamma\lambda[\cos(k_x) + \cos(k_y)]}$, each of which is doubly degenerate. The gap in the energy bands closes at $|\gamma/\lambda| = 1$. At half filling, when $|\gamma/\lambda| < 1$, the overall charge density is essentially localized at the corners of the open square lattice [see Figs. 4(a) and 4(b)], resulting in a nontrivial bulk quadrupole moment of the insulator [37]. On the other hand, when $|\gamma/\lambda| > 1$, both corner states and the quadrupole moment vanishes, and the insulator becomes trivial.

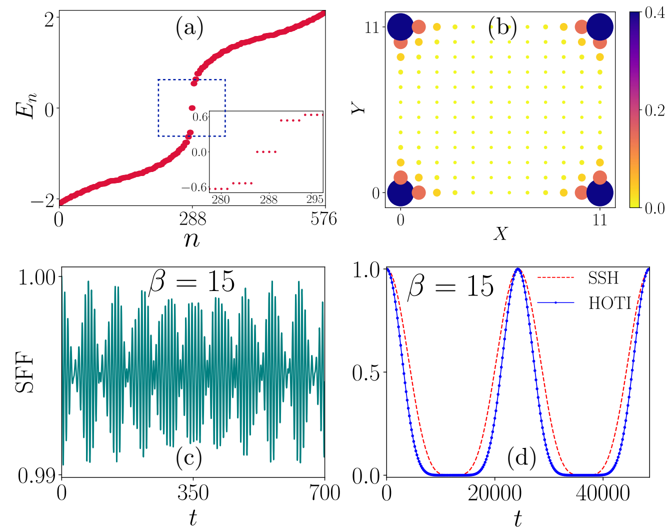


FIG. 4. (a) One-particle energy spectrum of the 2D HOTI model (see text; $\gamma = 0.5$, $\lambda = 1$) with the open boundary condition on a $12 \times 12$ lattice. The inset shows the four topological zero-energy modes. (b) Local probability density of the zero modes, showing that they are corner localized. (c) Plot of the SFF in the trivial regime ($\gamma = 1, \lambda = 0.5$). (d) Generalized Rabi oscillations in the topological regime of the HOTI (blue) ($\gamma = 0.5, \lambda = 1$) and the SSH system (red; $v = 0.5154$, $w = 1$, $L = 24$). The rise in the SFF in the former is $\sim t^8$ compared to $\propto t^4$ in the latter. In both (c) and (d) the SFF is calculated for $\beta = 15$.

Evaluating the SFF, we again find noisy oscillations in the trivial regime and long-time oscillations in the topological regime [see Figs. 4(c) and 4(d)]. Here, the effective many-body state spans $2^4$ states, which can be counted as occupancies of the four boundary modes. The oscillations follow

$$\text{SFF}(t) \sim [3 + 4\cos(\epsilon_a t) + \cos(2\epsilon_a t)]^2, \quad (13)$$

where $\epsilon_a$ is the exponentially small energy scale close to zero. Interestingly, the rise from zero is now $\sim t^8$, reflecting the higher number of zero modes in the system (see Fig. 4). In fact, for a multipole topological insulator [25] with a general number of $2p$ zero modes, the SFF would scale $\propto t^{4p}$ in the topological phase for $T < \Delta_g$. This is one of the key results of our work.

It is now natural to ask what the fate of such Rabi oscillations is in the presence of disorder, a question we answer next.

## IV. BULK-RANDOMIZED SSH SYSTEM

Motivated by random matrix theory (RMT), in which the symmetry properties of random dense Hamiltonian matrices determine their chaotic signatures [38–42], we introduce disorder to study the chaotic signatures in the SSH model, as discussed in the previous section. While generic short-range disorder in topological phases gives rise to a host of interesting phases and phase transitions [43–48], here, in order to simulate RMT chaos we introduce all-to-all hopping disorder

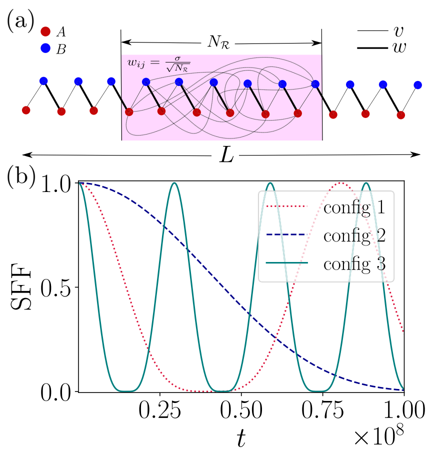


FIG. 5. (a) Schematic diagram of a bulk-random SSH chain [see Eq. (14)], where symmetry-preserved all-to-all hopping disorder is introduced in the central bulk region $\mathcal{R}$ with $N_{\mathcal{R}}$ sites of a clean open SSH chain [see Eq. (5)] of size $L$. The disordered hopping strengths $w_{ij}$ ($\{i, j\} \in \mathcal{R}$) are chosen from the Gaussian distribution with the scale parameter $\sigma/\sqrt{N_{\mathcal{R}}}$. (b) The SFF in the bulk-random SSH model ($L = 60$, $\beta = 50$, $\sigma = 0.1$, $N_{\mathcal{R}} = 30$) for different disorder configurations in the topological regime ($v = 0.5$, $w = 1$) shows long-time oscillations with different time periods.

simulating a “zero”-dimensional chaotic system in conjunction with an underlying topological phase.

To this effect, we mark a finite central region (excluding boundaries) in the bulk of the SSH chain [see Eq. (5)] as $\equiv \mathcal{R}$, where such hopping disorder is introduced (see Fig. 5). The microscopic Hamiltonian of such a system is

$$H_{\mathrm{R}} = H_{\mathrm{SSH}} - \sum_{\{i,j\}\in\mathcal{R}} (w_{ij}\, c^{\dagger}_{iA} c_{jB} + \mathrm{H.c.}). \tag{14}$$

Here, $w_{ij}$ are chosen from a Gaussian orthogonal ensemble with a scale parameter $\frac{\sigma}{\sqrt{N_{\mathcal{R}}}}$, where $N_{\mathcal{R}}$ is the number of sites in region $\mathcal{R}$ and $\{i, j\} \in \mathcal{R}$ [see Fig. 5(a)]. Since the disorder respects the sublattice character, given that $\mathcal{R}$ excludes the edges and $\sigma \ll |w - v|$, every disorder configuration will retain topologically protected zero modes. The numerical support for the stability of the topological phase with disorder strength and the length of the randomized region is given in Appendix A, where we show that, for small enough disorder strengths, the system described in Eq. (14) has quantized polarization. As every random realization of the disordered SSH chain is individually topological, the individual SFFs show long-time oscillations similar to a clean topological SSH chain [see Fig. 5(b)]. Since in this work we focus on disordered, but quadratic, systems in which the zero-energy manifold plays a crucial role, we do not investigate the effects of unfolding and filtering, which are designed to decipher many-body bulk chaotic signatures [49].

### A. SFF behavior

We find that the disorder-averaged SFF, irrespective of the topological character of the phase, has the following behavior as a function of time: (1) a dip, (2) an exponential oscillation and then a linear ramp, and (3) late-time saturation. The three regions are shown in Fig. 6(a). As one decreases the temperature (i.e., increases $\beta$), the exponential ramp starts to disappear [Fig. 6(b)]. For $\epsilon_0^{-1} \gg \beta > \Delta_g^{-1}$, the exponential ramp is almost entirely suppressed, and the late-time plateau value saturates around a new plateau value of $\sim 3/8 = 0.375$ instead of the usual plateau that scales as inverse of the system size (see Fig. 6).

At short times, the *exponentially* oscillating behavior is characteristic of signatures of single-particle chaos [16,17,26], which is in contrast to many-body chaos, which has a distinct linear ramp right after the dip [14,15]. To delve into an understanding of the different features of the SFF of the bulk-disordered SSH model, which is analytically intractable, one needs a simpler setting. To this end, we construct a minimal toy model, which we discuss next.

### B. Understanding using a toy system

In order to capture the physics of the disordered SSH model, we first explain the construction of an effective toy model. In Fig. 7, we plot the single-particle nearest-neighbor level spacings in the disordered SSH models, which show that they have a distribution similar to that of a Wigner-Dyson (WD) distribution. This motivates us to construct a toy model using the eigenvalues from GUE of random matrices, which has WD-distributed nearest-neighbor level spacings. This is also pertinent given that the nature of the ramp arises due

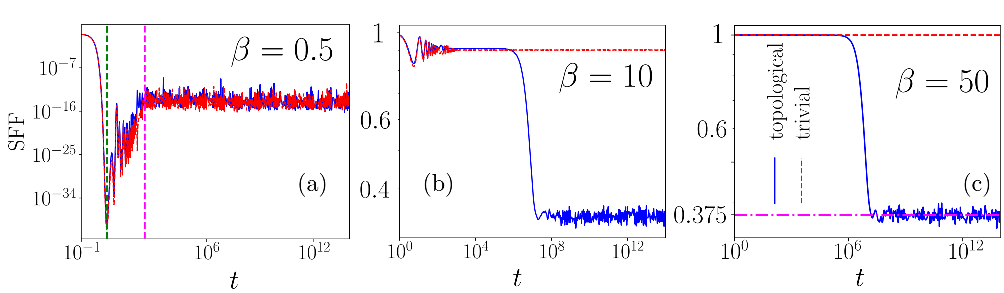


FIG. 6. (a) The SFF (disordered averaged over 2000 configurations) in the random SSH model ($L = 60$, $\beta = 0.50$, $\sigma = 0.01$, $N_{\mathcal{R}} = 30$) shows an early-time ramp in both the topological ($v = 0.5$, $w = 1$) and trivial ($v = 1$, $w = 0.5$) regimes. The green and magenta dashed vertical lines denote the dip time and plateau time calculated from the toy model. (b) With increasing $\beta$ ($= 10$), the initial dip starts to disappear, and a new plateau forms at a late time. (c) At very high $\beta$ ($= 50$), the early-time ramp disappears; the late-time plateau in the topological SFF saturates around 3/8. Here, $\Delta_g^{-1} \sim 2$, and $\epsilon_0^{-1} \sim 10^7$. Note that the trivial phase has saturated to a plateau value of unity.

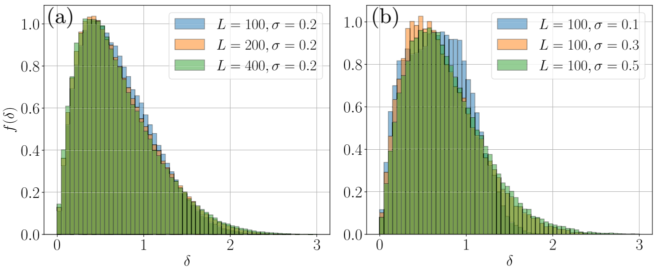


FIG. 7. Random SSH single-particle level spacing distributions (a) with the same randomness but different system sizes and (b) with the same system size but different randomness. Here, $v = 1$, and $w = 0.5$.

to the correlation between the level spacings of the spectrum [14].

The toy model consists of $N$ one-particle energy states taken from a GUE of random matrices which has semicircular $\rho(E)$ of radius $a$, centered around $a_{\max} = a + \Delta$ (with $\Delta > 0$) and a corresponding negative $E$ copy [see Fig. 8(a)]. The positive energy branch of the density of states (DOS) $\rho_+(E)$ is distributed between $a_1 = a_{\max} - a$ and $a_2 = a_{\max} + a$ with a spectral gap of $\Delta$. The ensemble-averaged $\rho_+(E)$ is given by

$$\langle \rho_+(E) \rangle = \frac{2}{a^2\pi}\sqrt{(E - a_1)(a_2 - E)}. \tag{15}$$

The ensemble-averaged SFF is then

$$\langle \mathcal{Z}_2^R(\beta, t) \rangle = \left\langle \exp\left(N \int dE\, \rho_+(E) \ln Z_2^E(\beta, t)\right)\right\rangle. \tag{16}$$

The angle brackets indicate the RMT averaging, in which all moments of $\rho_+(E)$ contribute. At early times, the disconnected piece dominates, leading to $\sim \exp\{[N \int dE\, \langle \rho_+(E)\rangle \ln Z_2^E(\beta, t)]\}$. Under a high-temperature expansion, the system exhibits the exponential ramp imbued with short-time oscillations. The $\beta \to 0$ limit is given by

$$\langle \mathcal{Z}_2^R(0, t) \rangle \approx \frac{\exp\left[8N \sum_{k=1}^{\infty} \frac{(-1)^{k+1}}{k^2 at} J_1(kat)\cos(ka_{\max}t)\right]}{16^N}. \tag{17}$$

In a microscopic model, $a_{\max}$ is the energy scale where the bulk DOS peaks. This points out that the location of the dip is set by the high energy scale $\pi/a_{\max} \sim t_{\text{dip}}$, which is both system size independent and is unaffected by its topological properties (see Fig. 6). The initial exponential oscillations lead to a linear ramp at $t_{\text{crossover}} \sim L^{2/3}$. This is a result of the leading connected piece, i.e., $\rho_c^{(2)}(E_1, E_2)$, becoming dominant, just as in the case of many-body SFF [14] (see Sec. B 1). The ramp further leads to a saturation, which can be remarkably different if the underlying system is trivial vs topological. More interestingly, the saturation physics is temperature dependent, as we now discuss.

At high temperatures ($T > |w - v|$), irrespective of topological features, the SFF saturates to a value dominated by the Kubo gap of the bulk spectra. This is essentially where all connected spectral correlations are featureless. For the minimal model, this predicts the emergence of a plateau at $t_{\text{plateau}} \sim 4N\pi$ (see Appendix B) and $\sim L$ for a bulk-disordered SSH system. However, now as $T$ is reduced below the bulk gap scale ($T < |w - v|$; see Fig. 2), depending on whether we are in the trivial or the topological phase, *another* saturation plateau appears.

This difference at low temperatures is due to the presence of zero-energy modes ($\sim \pm\epsilon_0$), which in the clean limit leads to large-time Rabi oscillations (see Fig. 2). The effective SFF can be captured in the form $\sim Z_2^{\epsilon_0}(\beta, t)\mathcal{Z}_2^R(\beta, t)$ [see Eq. (4)], where at low temperatures $Z_2^{\epsilon_0}$ dominates, and thus, any single configuration, even with bulk disorder, will lead to oscillations after a timescale $t^* \sim \frac{1}{\epsilon_0}$. However, the configuration-averaged SFF shows an intriguing behavior, as shown in Figs. 6(b) and 6(c). At low temperatures, the system reaches a *different* saturation value at later times. This central result, as we discuss next, is *not* governed by the large-$N$ RMT results but, rather, is governed by a small-$N$ RMT chaos.

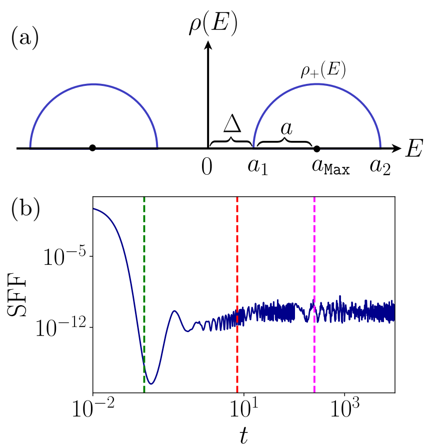


FIG. 8. (a) Toy model density of states. (b) Toy model ensemble-averaged SFF for $a_{\max} = 30$, $a = 20$, and $N = 20$. The green, red, and magenta lines denote $t_{\text{dip}}$, $t_{\text{crossover}}$, and $t_{\text{plateau}}$, respectively.

### C. Insights from random matrix theory

For the toy model discussed above with $N$ single-particle positive energy states, the late-time saturation value goes as $\sim 2^{-N}$ at $\beta = 0$, as can be seen directly from Eq. (4). As $\beta$ increases, for large enough $\beta$, the cosh $\beta\epsilon_n$ factor dominates in Eq. (4); thus, the plateau value approaches 1. However, for the bulk-random SSH chain, the SFF in the topological phase saturates at $\sim 3/8 = 0.375$, while the trivial phase SFF plateaus around 1 (see Fig. 6(b) and 6(c)). This indicates that in the trivial phase, i.e., in the absence of zero-energy boundary modes, the late-time saturation value is usually dictated by large-$N$ RMT chaos. On the contrary, the late-time saturation in the topological phase is an artifact of the chaos in the zero-energy manifold, which we denote as small-$N$ RMT chaos.

Every peripheral disorder realization in the region $\mathcal{R}$ perturbs the edge modes, which are, in turn, protected by the $(w, v)$ scale of the underlying SSH Hamiltonian. Therefore, at low energies, i.e., finite $\beta$ ($\beta > \Delta_g^{-1}$), the SFF gets dominated

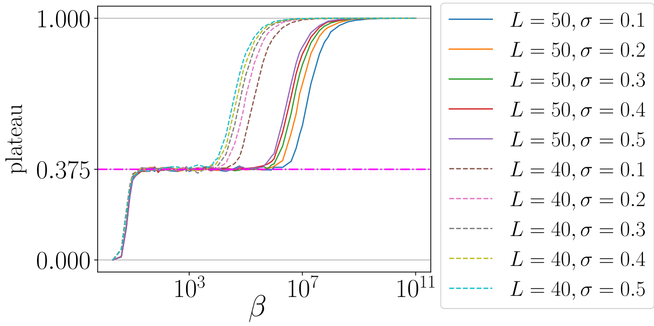


FIG. 9. Late-time ($t \sim 10^{12}$) saturation values for different system sizes $L$ and $\sigma$ plotted with respect to $\beta$ (here, $N_{\mathcal{R}} = L/2, v = 0.5, w = 1$). The SFFs are averaged over 2000 random configurations.

by RMTs reflecting the couplings within the zero-energy manifold itself. For instance, in the clean SSH model, the effective Hamiltonian in the context of our example is a single-qubit Hamiltonian $H_{\text{eff}} = \epsilon_0\sigma_x$, written in the left and right edge state basis ($|L\rangle, |R\rangle$). In the presence of disorder, each realization effectively introduces a perturbation in this overlap between the basis states; i.e., the single-qubit Hamiltonian now has an effective form: $H_{\text{eff}} = (\epsilon_0 + \lambda)\sigma_x$, where $\lambda$ can be considered to be drawn from a normalized Gaussian probability distribution $P(\lambda)$ distributed about the zero mean with a variance $\sigma$. This perturbation thus results in a Gaussian distribution of energy eigenvalues $\pm\epsilon_\lambda = \pm(\epsilon_0 + \lambda)$ centered around $\epsilon_0$ with variance $\sigma$. Thus, the averaged $Z_2^{\epsilon_0}(\beta, t)$ becomes

$$\langle\langle Z_2^{\epsilon_0}(\beta, t)\rangle\rangle = \int_{-\infty}^{\infty} d\lambda\, P(\lambda)\frac{[\cosh(\beta\epsilon_\lambda) + \cos(\epsilon_\lambda t)]^2}{[1 + \cosh(\beta\epsilon_\lambda)]^2}. \quad (18)$$

For the Gaussian distribution of $\epsilon_\lambda$ we obtain the long-time saturation value:

$$\lim_{t\to\infty} \langle\langle Z_2^{\epsilon_0}(\beta, t)\rangle\rangle \sim 3/8 \quad (19)$$

when $\epsilon_0 \ll T < |w - v|$ or, equivalently, $\Delta_g^{-1} \ll \beta \ll \epsilon_0^{-1}$. Thus, this late-time behavior in the topological phase is fundamentally distinct from the trivial regime, where no such zero-energy manifold exists, and the SFF just saturates to 1. Note that the long-time saturation value is independent of the system size and microscopic parameters, as indicated by the numerical results in Fig. 9. Further lowering of temperature ($T < \epsilon_0$), even in the topological phase, drives the plateau towards unity as well. This is clear from Eq. (18), as for large $\beta$ we obtain

$$\langle\langle Z_2^{\epsilon_0}(\beta, t)\rangle\rangle \simeq \int_{-\infty}^{\infty} d\lambda\, P(\lambda) = 1. \quad (20)$$

The analytical predictions exactly match our numerical results, as shown in Fig. 6(b). For further details of the SFF calculations, see Sec. B 2.

This result can be further generalized for a topological phase containing $p$ pairs of symmetric zero modes: $\{\epsilon_0^{(1)}, -\epsilon_0^{(1)}\}, \{\epsilon_0^{(2)}, -\epsilon_0^{(2)}\}, \ldots, \{\epsilon_0^{(p)}, -\epsilon_0^{(p)}\}$. In this case, under bulk disorder, each zero-energy pair can be thought to arise from a single-qubit effective Hamiltonian $H_{\text{eff}}^{(j)} = \epsilon_0^{(j)}\sigma_z + \lambda_j\sigma_x$ with energy eigenvalues $\epsilon_\lambda^{(j)} = \sqrt{(\epsilon_0^{(j)})^2 + \lambda_j^2}$. Here, $\lambda_j$ is drawn from some normalized probability distribution $P_j(\lambda_j)$. Under the assumption that all zero-energy pair fluctuations are mutually independent, the effective Hamiltonian of the zero-energy manifold is then

$$H_{\text{eff}}^0 = \bigotimes_{j=1}^{p} H_{\text{eff}}^{(j)}.$$

Then for a Gaussian distribution of $\epsilon_\lambda^{(j)}$ centered around $\epsilon_0^{(j)}$, the average zero-energy SFF is

$$\left\langle\left\langle \prod_{j=1}^{p} Z_2^{\epsilon_0^{(j)}}(\beta, t)\right\rangle\right\rangle \xrightarrow{t\to\infty} (3/8)^p. \quad (21)$$

This is the long-time plateau value of the SFF for the topological phase in the regime $\Delta_g^{-1} \ll \beta \ll \epsilon_0^{-1}$. Note that the bulk-disordered SSH model is the $p = 1$ case, as it contains only one pair of zero-energy modes. We note, however, that the effective nature of hybridization within the effective zero-energy manifold may depend on the system and symmetries of the microscopic model.

## V. CONCLUSIONS

In this work, we showed that underlying topological order has important implications for chaotic signatures in quantum systems. Our analysis established that the emergence of zero-energy boundary modes fundamentally changes the late-time behavior of the SFF, a versatile tool that has been critical for diagnosing chaos and thermalization in a host of systems. In Sec. II, we explored the idea of the spectral form factor, its general features, and how it is evaluated for a noninteracting system. We then discussed that in a clean topological system, the SFF shows oscillations akin to generalized Rabi oscillations with features characteristic of the underlying topological properties. In particular, we studied the behavior of the SFF in the SSH and HOTI models, in which the system hosts zero-dimensional edge modes (Sec. III). In order to study the interplay with signatures of single-particle chaos we introduced disorder in such a way that the edge modes remain intact. In particular, we introduced symmetry-preserved all-to-all hopping disorder in the bulk of an SSH chain (Sec. IV). Interestingly, we found that bulk disorder alters the late-time SFF plateau in a topological phase. Gathering intuition from both numerical results and analytical calculations for effective toy models, our study uncovered the physics that the late-time plateau is, in fact, determined by RMT behavior within the zero-energy manifold.

While our work has investigated the role of noninteracting topology on the SFF, we have restricted ourselves to systems in which the topological manifold provides zero modes such as in SSH or HOTI systems. Here, the separation of scales between the boundary manifold and bulk manifold is relatively clear. Even within symmetry-protected topological phases and higher-dimensional topological phases such as Chern insulators and topological insulators [21,23], it may be interesting to explore how this physics changes. Here, the eigenspectrum related to the boundary smoothly merges with the bulk spectrum, thus making the physics more interesting. Another

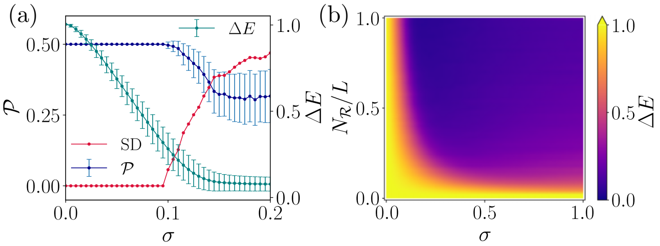


FIG. 10. (a) The polarization $\mathcal{P}$ shows the stability of the topological phase up to a critical $\sigma$ for the SSH Hamiltonian with the 90% bulk region having all-to-all random hopping. The stability can also be seen from the standard deviation (SD) of the polarization, which is clearly related to the closing of the bulk gap $\Delta E$ in the system. (b) Contour plot of the bulk gap with the disorder strength $\sigma$ and the fraction of random sites $N_{\mathcal{R}}/L$. For both the plots, the system size is $L = 100$, $v = 0.5$, $w = 1$, and all the data are averaged over 1000 random configurations.

natural question to pose what the role of both interactions and long-range topological order is. Under both repulsive and attractive perturbative interactions, the SSH model is known to be stable and retains fourfold degenerate boundary modes in its many-body spectrum [50–52]. Thus, we expect the SFF to have long-time oscillations as long as the interaction does not close the bulk gap in the system. However, an elaborate study of the SFF in interacting SSH and higher-dimensional topological phases is an exciting future prospect.

## ACKNOWLEDGMENTS

A.S. and S.P. acknowledge funding from IIT Kanpur. A.A. acknowledges support from IIT Kanpur Initiation Grant No. IITK/PHY/2022010. D.D. and A.S. acknowledge support from Max Planck Partner Group Grant No. MAXPLA/PHY/2018577. D.D. acknowledges support from MATRICS Grant No. SERB/PHY/2020334. We acknowledge fruitful discussions at the "Discussion Meeting on Non-equilibrium Correlated Systems" held at HRI, Allahabad.

## APPENDIX A: STABILITY TO DISORDER

In any topological phase, the presence of a bulk gap and underlying symmetries protects the boundary modes under perturbative disorder. In our work, directed towards studying the role of topological boundary modes in the SFF, we show that even in the presence of all-to-all random hopping (drawn from a Gaussian distribution with zero mean and variance $\sigma$) in a finite region $\mathcal{R}$, the boundary modes remain stable until a finite $\sigma$. We study *polarization*, which is the real-space representation of the topological invariant (winding number) in one-dimensional systems [53]. The polarization is defined as

$$\mathcal{P} = \frac{1}{2\pi}\mathrm{Im}\{\mathrm{Tr}[\ln(\hat{P}D\hat{P})]\} \mod 1, \tag{A1}$$

where $\hat{P} = \sum_{E_n \leqslant E_F} |\psi_n\rangle\langle\psi_n|$ is the ground state projection operator, with $|\psi_n\rangle$ being the single-particle eigenstate corresponding to the energy eigenvalue $E_n$ and $E_F$ being the Fermi energy of the system. The positions $x_i$ of all the lattice sites (for system size $L$ there are $N = L/2$ unit cells) are compactified and exponentiated to give the operator $D = \mathrm{diag}[e^{2\pi x_{i\alpha}/N}]$, where $x_{i\alpha} = (i-1)$ for the $i$th unit cell and both $\alpha = A, B$ sublattices. In the absence of disorder, in the topological regime of the SSH Hamiltonian ($|v/w| < 1$), the polarization $\mathcal{P}$ is quantized to 0.5, while it is zero for the trivial insulating phase ($|v/w| > 1$). Furthermore, in Fig. 10(a) we plot the polarization [see Eq. (A1)] of the system in the topological regime ($v/w = 0.5$) as a function of bulk disorder $\sigma$ in 90% ($N_{\mathcal{R}}/L = 0.9$) of bulk sites. The system shows quantized polarization as well as a finite bulk gap $\Delta E$ up to a finite $\sigma$, confirming that the system's topological properties remain stable even when bulk disorder randomizes the bulk spectra. Furthermore, the stability increases as the number of bulk sites disordered is reduced; see Fig. 10(b), where the bulk gap is plotted as a function of $N_{\mathcal{R}}/L$ and $\sigma$.

## APPENDIX B: ADDITIONAL DETAILS OF SFF CALCULATIONS

### 1. Toy model for bulk disorder

Here, we go through a detailed analysis of the bulk-disordered toy model described earlier.

The many-body SFF, when ensemble averaged, is given by $\langle Z_2^R(\beta,t)\rangle$,

$$\langle \mathcal{Z}_2^R(\beta,t)\rangle = \left\langle \exp\left(N\int \mathrm{d}E\,\rho_+(E)\,\ln Z_2^E\right)\right\rangle = \sum_{n=0}^{\infty}\frac{1}{n!}N^n\int\left(\prod_{i=1}^{n}\mathrm{d}E_i\right)\langle\rho_+(E_1)\cdots\rho_+(E_n)\rangle\prod_{j=1}^{n}\ln Z^{E_j}(\beta,t), \tag{B1}$$

where a typical $n$-point density correlator has the form

$$\langle\rho_+(E_1)\cdots\rho_+(E_n)\rangle \equiv \langle\rho^{(n)}\rangle = \prod_{i=1}^{n}\langle\rho_i^{(1)}\rangle + \sum_{\{n_i,m\}}A^{\{n_i,m\}}\prod_{i=1}^{k}\rho_c^{(n_i)}\prod_{j}^{m}\langle\rho_j^{(1)}\rangle,\ \sum_{\substack{i=1\\ n_i>1}}^{k}n_i + m = n,\ \sum_{i}^{k}n_i \neq 0. \tag{B2}$$

Here, the first term denotes the disconnected piece, $A^{\{n_i,m\}}$ stands for the coefficient arising from the permutations of the indices, $\rho_c^{(n_i)}$ denotes the completely connected piece of the $n_i$-point correlation, and $\rho_j^{(1)} \equiv \rho_+(E_j)$.

Using the explicit form for the joint distributions, as given by the determinant of the kernel [31], we find

$$\prod_{i=1}^{n}\langle\rho_i^{(1)}\rangle = O(1),\ \ \prod_{i=1}^{k}\rho_c^{(n_i)}\prod_{j}^{m}\langle\rho_j^{(1)}\rangle = O(N^{m-n}) = O(N^{-\sum_i n_i}). \tag{B3}$$

Since $\min(n_i) \geqslant 2$, the second term is always at least $O(1/N^2)$ suppressed compared to the fully disconnected one. Of course, after evaluating the integrals in (B1), there are nontrivial time growths associated with various pieces. At early times, $t \ll N$, we can ignore these time dependences, and the dominant contribution, at large $N$, comes from the fully disconnected DOS correlator. Therefore, the sum over $n$ in Eq. (B1) reexponentiates, and we find the early-time, ensemble-averaged SFF is

$$\left\langle \mathcal{Z}_2^R(\beta, t)\right\rangle \simeq \exp\left(N\int \mathrm{d}E\,\langle\rho_+(E)\rangle\,\ln Z_2^E\right) = \exp\left(N\int_{a_1}^{a_2}\mathrm{d}E\,\frac{2}{a^2\pi}\sqrt{(E-a_1)(a_2-E)}\,\ln Z_2^E\right). \tag{B4}$$

At high temperatures, $\beta = 0$, the integral can be evaluated exactly in terms of the Bessel function:

$$\left\langle \mathcal{Z}_2^R(0, t)\right\rangle \simeq \frac{1}{16^N}\exp\left(8N\sum_{k=1}^{\infty}\frac{(-1)^{k+1}}{k^2 at}J_1(kat)\cos(ka_{\max}t)\right). \tag{B5}$$

In the above expression, the higher-frequency oscillations $\cos(ka_{\max}t)$ are suppressed as $k^{-2}$. Thus, the $k=1$ component dominates and produces the dip at the first oscillation minimum: $t_{\rm dip} = \pi/a_{\max}$.

To see the dynamics at an intermediate time, we look at the connected component of $\langle\rho_+(E_1)\rho_+(E_2)\rangle$, denoted as $\rho_c^{(2)}(E_1, E_2)$. In terms of the sine kernel [14], from Eq. (B1) we obtain

$$\begin{aligned}
&\frac{1}{2!}N^2\int \mathrm{d}E_1\mathrm{d}E_2\,\rho_c^{(2)}(E_1,E_2)\prod_{j=1}^{2}\ln Z_2^{E_j}\\
&= -\frac{N^2}{2!}\int \mathrm{d}E_1\mathrm{d}E_2\,\frac{\sin^2[N\pi(E_1-E_2)]}{N^2\pi^2(E_1-E_2)^2}\prod_{j=1}^{2}\ln Z_2^{E_j}\\
&= -\frac{2}{\pi}\Bigg\{N\pi\,\ln^2(4) - \ln(4)\sum_{k=1}^{\infty}\frac{(-1)^{k+1}}{k}(4N\pi - kt)\cos(ka_{\max}t)\Theta\left(\frac{4N\pi}{k}-t\right)\\
&\quad + \sum_{k,l=1}^{\infty}\frac{(-1)^{k+l}}{kl}\Bigg[[4N\pi-(k+l)t]\cos(|k-l|a_{\max}t)\Theta\left(\frac{4N\pi}{(k+l)}-t\right)\\
&\quad + (4N\pi - |k-l|t)\cos[(k+l)a_{\max}t]\Theta\left(\frac{4N\pi}{|k-l|}-t\right)\Bigg]\Bigg\}.
\end{aligned} \tag{B6}$$

We see the two-point connected piece generates linear terms of $(4N\pi - kt)$ up to $t = 4N\pi/k$. Thus, the $k=1$ component gives the longest surviving linear piece with the plateau time $t_{\rm plateau} = 4N\pi$ [see Fig. 8(b)].

Comparing the disconnected and connected pieces for $n = 2$, we can estimate the time $t_{\rm crossover}$ at which the connected piece starts to dominate over the disconnected piece. Using the asymptotic form of Bessel functions, we find

$$N^2\frac{J_1(t_{\rm crossover})}{t_{\rm crossover}} \sim N \;\Rightarrow\; t_{\rm crossover} \sim O(N^{2/3}). \tag{B7}$$

So we see a linear ramp starting from $t_{\rm crossover}$ up to $t_{\rm plateau}$, and then the SFF plateaus.

As we see from the $n=2$ case, the surviving piece in long-time average is $\sim O(N)$ for the connected piece, while the disconnected piece has a long-time average value of $\sim O(N^2)$. Thus, in all $n$-point correlations, the disconnected piece gives the dominant long-time average contribution. From Eq. ((B5)), we see in the long-time average the oscillations die down; thus, the plateau value becomes

$$\left\langle \mathcal{Z}_2^R(0, t\to\infty)\right\rangle \sim e^{-N}. \tag{B8}$$

### 2. Late-time SFF dynamics due to fluctuating zero modes

In the one-dimensional SSH model, there are two zero modes with energy $\pm\epsilon_0$ at the two ends of the lattice chain. When disorder is introduced in the bulk, the zero modes also fluctuate. To model the spectrum of these two fluctuating zero modes, we consider a Gaussian energy distribution centered around $\epsilon_0$ with the variance $\sigma$. Thus, the ensemble-averaged zero-energy contribution to the SFF is

$$\left\langle\left\langle Z_2^{\epsilon_0}(\beta, t)\right\rangle\right\rangle = \int \mathrm{d}\epsilon\,\frac{1}{\sigma\sqrt{2\pi}}e^{-\frac{(\epsilon-\epsilon_0)^2}{2\sigma^2}}\left(\frac{\cosh(\beta\epsilon)+\cos(\epsilon t)}{\cosh(\beta\epsilon)+1}\right)^2. \tag{B9}$$

For $\beta = 0$ (i.e., $\beta \ll \epsilon_0^{-1}$) we have

$$\begin{aligned}
\langle\langle Z_2^{\epsilon_0}(0,t)\rangle\rangle &= \frac{1}{\sigma\sqrt{2\pi}}\int \mathrm{d}\epsilon\, e^{-\frac{(\epsilon-\epsilon_0)^2}{2\sigma^2}}\left(\frac{1+\cos(\epsilon t)}{2}\right)^2\\
&= \frac{3}{8} + \frac{1}{2}e^{-t^2\sigma^2/2}\cos(\epsilon_0 t) + \frac{1}{8}e^{-2t^2\sigma^2}\cos(2\epsilon_0 t).
\end{aligned} \tag{B10}$$

At large $t$, the oscillations will average to zero, thus leading to a plateau value of $3/8 = 0.375$.

To calculate the dip point, we can find the first minimum of $\langle\langle Z_2^{\epsilon_0}(0,t)\rangle\rangle$ [ignoring the $\cos(2\epsilon_0 t)$ term] and arrive at the transcendental equation

$$\partial_t \langle\langle Z_2^{\epsilon_0}(0,t)\rangle\rangle = 0 \Rightarrow \tan(\epsilon_0 t) = -\frac{t\sigma^2}{\epsilon_0}. \tag{B11}$$

When $\sigma \ll \epsilon_0$, in the above expression $\tan(\epsilon_0 t_{\rm dip}) \to 0$; thus, $t_{\rm dip} \to \frac{\pi}{\epsilon_0}$. In this case, the exponential $\sim e^{-t^2\sigma^2/2}$ decay does not sufficiently suppress the $\cos(\epsilon_0 t)$ oscillations; thus, we see an oscillatory dip-ramp and plateau. For $\sigma \gg \epsilon_0$, $\tan(\epsilon_0 t_{\rm dip}) \to -\infty$; hence, $t_{\rm dip} \to \frac{\pi}{2\epsilon_0}$. In this case, the exponential decay dominates. Thus, we see only a dip and plateau, without any ramp. In the actual random SSH model, we have both the random excited states and fluctuating zero modes, i.e., $\langle \mathcal{Z}_2^{\rm Full}(\beta,t)\rangle = \langle \mathcal{Z}_2^R(\beta,t)\rangle\langle\langle Z_2^{\epsilon_0}(\beta,t)\rangle\rangle$. Thus, when $\epsilon_0^{-1} \gg \beta > \Delta^{-1}$, the early-time dip-ramp due to $\langle \mathcal{Z}_2^R(\beta,t)\rangle$ starts to get suppressed, and we start to see the late-time SFF dynamics of $\langle\langle Z_2^{\epsilon_0}(\beta,t)\rangle\rangle$ (see Fig. 6).


[1] M. Srednicki, Chaos and quantum thermalization, Phys. Rev. E **50**, 888 (1994).

[2] L. D'Alessio, Y. Kafri, A. Polkovnikov, and M. Rigol, From quantum chaos and eigenstate thermalization to statistical mechanics and thermodynamics, Adv. Phys. **65**, 239 (2016).

[3] F. Borgonovi, F. M. Izrailev, L. F. Santos, and V. G. Zelevinsky, Quantum chaos and thermalization in isolated systems of interacting particles, Phys. Rep. **626**, 1 (2016).

[4] A. Das, S. Chakrabarty, A. Dhar, A. Kundu, D. A. Huse, R. Moessner, S. S. Ray, and S. Bhattacharjee, Light-cone spreading of perturbations and the butterfly effect in a classical spin chain, Phys. Rev. Lett. **121**, 024101 (2018).

[5] J. Pollack, M. Rozali, J. Sully, and D. Wakeham, Eigenstate thermalization and disorder averaging in gravity, Phys. Rev. Lett. **125**, 021601 (2020).

[6] S. D. Murugan, D. Kumar, S. Bhattacharjee, and S. S. Ray, Many-body chaos in thermalized fluids, Phys. Rev. Lett. **127**, 124501 (2021).

[7] J. S. Cotler, G. Gur-Ari, M. Hanada, J. Polchinski, P. Saad, S. H. Shenker, D. Stanford, A. Streicher, and M. Tezuka, Black holes and random matrices, J. High Energy Phys. 05 (2017) 118; Erratum to: Black holes and random matrices, *ibid.* 09 (2018) 002.

[8] P. Saad, S. H. Shenker, and D. Stanford, A semiclassical ramp in SYK and in gravity, arXiv:1806.06840.

[9] E. Dyer and G. Gur-Ari, 2D CFT partition functions at late times, J. High Energy Phys. 08 (2017) 075.

[10] Nivedita, H. Shackleton, and S. Sachdev, Spectral form factors of clean and random quantum Ising chains, Phys. Rev. E **101**, 042136 (2020).

[11] A. del Campo, J. Molina-Vilaplana, and J. Sonner, Scrambling the spectral form factor: Unitarity constraints and exact results, Phys. Rev. D **95**, 126008 (2017).

[12] I. Bena, M. Droz, and A. Lipkowski, Statistical mechanics of equilibrium and nonequilibrium phase transitions: The Yang-Lee formalism, Int. J. Mod. Phys. B **19**, 4269 (2005).

[13] A. W. Harrow, S. Mehraban, and M. Soleimanifar, Classical algorithms, correlation decay, and complex zeros of partition functions of quantum many-body systems, in *Proceedings of the 52nd Annual ACM SIGACT Symposium on Theory of Computing* (Association for Computing Machinery, New York, NY, 2020).

[14] J. Cotler, N. Hunter-Jones, J. Liu, and B. Yoshida, Chaos, complexity, and random matrices, J. High Energy Phys. 11 (2017) 048.

[15] J. Liu, Spectral form factors and late time quantum chaos, Phys. Rev. D **98**, 086026 (2018).

[16] M. Winer, S.-K. Jian, and B. Swingle, An exponential ramp in the quadratic Sachdev-Ye-Kitaev model, Phys. Rev. Lett. **125**, 250602 (2020).

[17] Y. Liao, A. Vikram, and V. Galitski, Many-body level statistics of single-particle quantum chaos, Phys. Rev. Lett. **125**, 250601 (2020).

[18] J. Kudler-Flam, L. Nie, and S. Ryu, Conformal field theory and the web of quantum chaos diagnostics, J. High Energy Phys. 01 (2020) 175.

[19] A. W. W. Ludwig, Topological phases: Classification of topological insulators and superconductors of non-interacting fermions, and beyond, Phys. Scr. **T168**, 014001 (2016).

[20] C.-K. Chiu, J. C. Y. Teo, A. P. Schnyder, and S. Ryu, Classification of topological quantum matter with symmetries, Rev. Mod. Phys. **88**, 035005 (2016).

[21] M. Z. Hasan and C. L. Kane, Colloquium: Topological insulators, Rev. Mod. Phys. **82**, 3045 (2010).

[22] X.-L. Qi and S.-C. Zhang, Topological insulators and superconductors, Rev. Mod. Phys. **83**, 1057 (2011).

[23] J. K. Asbóth, L. Oroszlány, and A. Pályi, *A Short Course on Topological Insulators*, Lecture Notes in Physics Vol. 919 (Springer, Cham, 2016), p. 166.

[24] W. P. Su, J. R. Schrieffer, and A. J. Heeger, Solitons in polyacetylene, Phys. Rev. Lett. **42**, 1698 (1979).

[25] W. A. Benalcazar, B. A. Bernevig, and T. L. Hughes, Quantized electric multipole insulators, Science **357**, 61 (2017).

[26] Y. Chen, Spectral form factor for free large N gauge theory and strings, J. High Energy Phys. 06 (2022) 137.

[27] R. E. Prange, The spectral form factor is not self-averaging, Phys. Rev. Lett. **78**, 2280 (1997).

[28] E. Brézin and S. Hikami, Spectral form factor in a random matrix theory, Phys. Rev. E **55**, 4067 (1997).

[29] G. Cipolloni, L. Erdős, and D. Schröder, On the spectral form factor for random matrices, Commun. Math. Phys. **401**, 1665 (2023).

[30] P. Sierant, D. Delande, and J. Zakrzewski, Thouless time analysis of anderson and many-body localization transitions, Phys. Rev. Lett. **124**, 186601 (2020).

[31] E. Brezin and A. Zee, Universality of the correlations between eigenvalues of large random matrices, Nucl. Phys. B **402**, 613 (1993).

[32] M. L. Mehta, *Random Matrices*, 3rd ed. (Academic Press, 2004).

[33] A. Altland and M. R. Zirnbauer, Nonstandard symmetry classes in mesoscopic normal-superconducting hybrid structures, Phys. Rev. B **55**, 1142 (1997).

[34] A. Agarwala, A. Haldar, and V. B. Shenoy, The tenfold way redux: Fermionic systems with n-body interactions, Ann. Phys. (NY) **385**, 469 (2017).
[35] J. J. Sakurai, *Modern Quantum Mechanics*, revised ed. (Pearson Education India, 1967).
[36] D. J. Griffiths and D. F. Schroeter, *Introduction to Quantum Mechanics* (Cambridge University Press, Cambridge, 2018).
[37] B. Kang, K. Shiozaki, and G. Y. Cho, Many-body order parameters for multipoles in solids, Phys. Rev. B **100**, 245134 (2019).
[38] F. J. Dyson, Statistical theory of the energy levels of complex systems. I, J. Math. Phys. **3**, 140 (1962).
[39] B. Bertini, P. Kos, and T. Prosen, Exact spectral form factor in a minimal model of many-body quantum chaos, Phys. Rev. Lett. **121**, 264101 (2018).
[40] A. Chan, A. De Luca, and J. T. Chalker, Spectral statistics in spatially extended chaotic quantum many-body systems, Phys. Rev. Lett. **121**, 060601 (2018).
[41] M. Tezuka, O. Oktay, E. Rinaldi, M. Hanada, and F. Nori, Binary-coupling sparse Sachdev-Ye-Kitaev model: An improved model of quantum chaos and holography, Phys. Rev. B **107**, L081103 (2023).
[42] P. Kos, M. Ljubotina, and T. Prosen, Many-body quantum chaos: Analytic connection to random matrix theory, Phys. Rev. X **8**, 021062 (2018).
[43] O. Balabanov and H. Johannesson, Robustness of symmetry-protected topological states against time-periodic perturbations, Phys. Rev. B **96**, 035149 (2017).
[44] T. Liu and H. Guo, Topological phase transition in the quasiperiodic disordered Su-Schriffer-Heeger chain, Phys. Lett. A **382**, 3287 (2018).
[45] E. J. Meier, F. A. An, A. Dauphin, M. Maffei, P. Massignan, T. L. Hughes, and B. Gadway, Observation of the topological anderson insulator in disordered atomic wires, Science **362**, 929 (2018).
[46] S. Longhi, Topological Anderson phase in quasi-periodic waveguide lattices, Opt. Lett. **45**, 4036 (2020).
[47] X. Shi, I. Kiorpelidis, R. Chaunsali, V. Achilleos, G. Theocharis, and J. Yang, Disorder-induced topological phase transition in a one-dimensional mechanical system, Phys. Rev. Res. **3**, 033012 (2021).
[48] Z.-W. Zuo and D. Kang, Reentrant localization transition in the Su-Schrieffer-Heeger model with random-dimer disorder, Phys. Rev. A **106**, 013305 (2022).
[49] J. Šuntajs, J. Bonča, T. Prosen, and L. Vidmar, Quantum chaos challenges many-body localization, Phys. Rev. E **102**, 062144 (2020).
[50] M. Kohmoto, M. den Nijs, and L. P. Kadanoff, Hamiltonian studies of the $d = 2$ Ashkin-Teller model, Phys. Rev. B **24**, 5229 (1981).
[51] A. Prakash, M. Fava, and S. A. Parameswaran, Multiversality and unnecessary criticality in one dimension, Phys. Rev. Lett. **130**, 256401 (2023).
[52] S. Mondal, A. Agarwala, T. Mishra, and A. Prakash, Symmetry-enriched criticality in a coupled spin ladder, Phys. Rev. B **108**, 245135 (2023).
[53] R. Resta, Quantum-mechanical position operator in extended systems, Phys. Rev. Lett. **80**, 1800 (1998).